First physics results from the HARP experiment at CERN

A. Cervera Villanueva
University of Geneva, Switzerland

The first physics results of the HARP experiment are presented. We emphasize the high performance of the forward part of the apparatus. The differential raw pion yield and its efficiency correction up to polar angles of 250 *mrad* are shown. The analysed setting is 12.9 GeV/c incident protons in a 5% interacion legth aluminium target.

1 Introduction

The HARP experiment [1] was designed to perform a systematic and precise study of hadron production for beam momenta between 1.5 and 15 GeV/c , for target nuclei ranging from hydrogen to lead. The detector was located at CERN, in the PS beam, and took 420 million events during the years 2001 and 2002.

The physics goals of HARP are to make a measurement of the pion yield that will enable a quantitative design of the proton driver of a neutrino factory, and to improve the precision of atmospheric neutrino flux calculations. In addition, the energy-range is suitable to measure particle yields for the prediction of neutrino fluxes for the MiniBooNE [4] and K2K [5] experiments (8.9 and 12.9 GeV/c respectively). To this end a collaboration was set up with these groups. Beam energy settings and dedicated targets were used to provide the most relevant measurements.

A schematic layout of the apparatus is shown in Fig. 1. It is a large acceptance spectrometer, with two distinct regions. A forward region (up to polar angles of about 250 *mrad*), where the main tracking devices are a set of drift chambers, and where particle identification is possible thanks to the combination of a threshold cerenkov, a time-of-flight wall and an electron identifier. In the large-angle region the main tracking and particle-id detector is a TPC, which is complemented by a set of RPC detectors for time of flight measurements. In addition, a complex beam instrumentation was set up in order to establish the nature of the incoming particle,

given the rather impure beam. The main subsystems are three small timing detectors and two cerenkovs. The beam time detectors are also used to estimate the interaction time at the target, located inside the TPC.

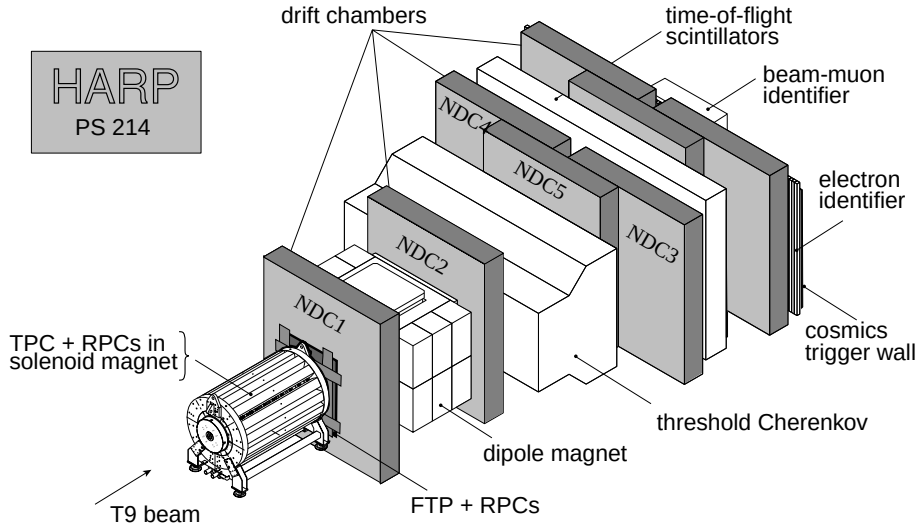

Figure 1: Schematic layout of the HARP spectrometer.

Given the immediate interest of the MiniBooNE and K2K experiments in our results, the HARP Collaboration has decided to start the data analysis with these two attractive items. In particular, we present in this article a first analysis of the data dedicated to the K2K measurement, using for this purpose the forward region of the detector, which is able to cover by itself the K2K requirements.

The organisation is as follows. Section 2 introduces the motivation of this analysis. In section 3 the tracking capabilities of the forward spectrometer are presented. Section 4 is devoted to the particle identification subsystems and their performance. Finally, the data analysis is presented in section 5 and the conclusions in section 6.

2 Motivation of this analysis

One of the main systematic errors on the neutrino oscillation parameters measured by the K2K experiment comes from the uncertainty on the far/near neutrino flux ratio. This ratio depends on the differential pion production cross section, which is essentially measured by a threshold cerenkov (pion monitor) above $E_\nu = 1\ GeV$, but must rely on Monte Carlo simulations below that energy. Unfortunately, the oscillation peak is located at $E_\nu \sim 0.55\ GeV$. HARP could precisely estimate the pion differential cross section at these energies and subsequently reduce that systematic error.

Fig. 2-left shows the (p, θ) distribution for pions producing neutrinos in the bin containing the oscillation peak ($0.5-0.75\ GeV$). The relevant phase space is $1<p<8\ GeV$ and $\theta<250\ mrad$, which is fully covered by HARP's forward region as shown in Fig. 2.

3.5 million useful events were taken by HARP with incident 12.9 GeV/c protons and an exact replica of the K2K target, which is a $80 \times 3\ cm$ aluminum tube (2 interaction lengths). Another 6M events were collected with a $5\%\lambda$ aluminium target ("K2K thin target") and a similar beam in order to decouple reinteraction and absorption effects from pure production. The data analysis presented in this article is based on this particular setting.

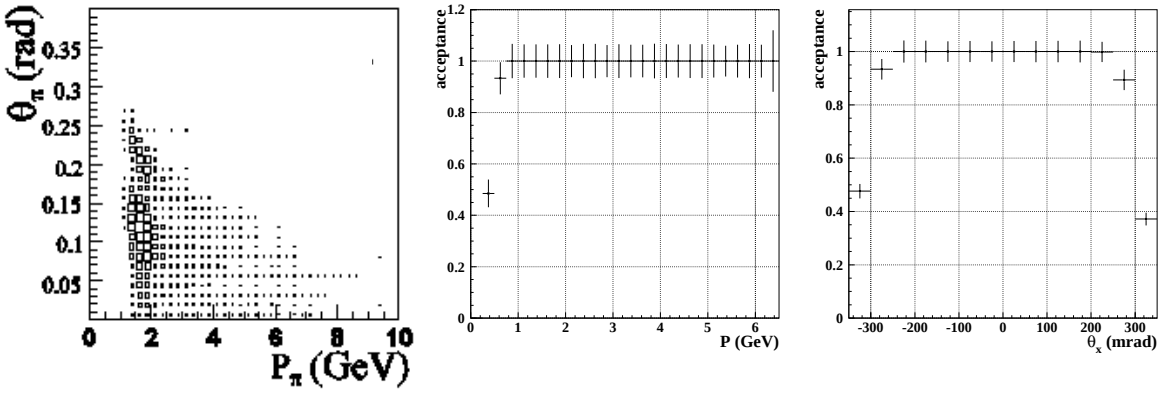

Figure 2: On the left, (p, θ) distribution for pions producing neutrinos in the bin containing the oscillation peak $(0.5 - 0.75\ GeV)$. This figure is a courtesy of the K2K Collaboration. It has been obtained with a full simulation of the K2K pion production and decay chains. Center and right, geometrical acceptance of HARP's dipole magnet for particles arriving to the first NDC module (NDC1). On the center, P dependence for particles with $|\theta_x| < 200\ mrad$. On the right, θ_x dependence for particles with $P > 1\ GeV/c$.

3 Forward Tracking

Tracking of forward going particles is done by a set of drift chambers (NDC) placed upstream and downstream of the dipole magnet (DIP). The NDC-DIP combination allows the momentum measurement by matching track segments located at either side of the magnet.

The chambers were recuperated from the NOMAD experiment and their properties have been described elsewhere [2]. Each NDC module contains 4 chambers, and each chamber 3 planes of wires with tilted angles -5^o, 0^o and 5^o. The single wire efficiency is of the order of 80%, and the spatial resolution approximately 340 μm. [a]

The reconstruction algorithm builds $2D$ and $3D$ track segments in each NDC module (12 hits maximum), which are fitted to a straight line model via a Kalman Filter fit [6]. Afterwards, all the possible matching combinations of tracking objects (including unused hits) belonging to different modules are performed in order to obtain longer tracks.

The momentum measurement is done associating $3D$ downstream segments with $3D$ and $2D$ segments in the upstream module (NDC1). This asymmetry is needed to compensate the low tracking efficiency of the upstream chambers, due to the presence of a unique module and to the higher hit density (proximity to the target), which provokes pattern recognition confusion. Fig. 4 shows the momentum and angular resolutions for $3D$-$3D$ up-down matches.

The small track separation in NDC1 induces a huge correlation between particles that implies a hadron model dependent tracking efficiency. This is a potential source of systematic error as shown in Fig. 3. The average efficiency is of the order of 65% when one consideers only $3D$-$3D$ up-down matches. The situation improves when $2D$-$3D$ matches are included. Recent studies with a third type of tracks, built by matching a $3D$ downstream track with the vertex, show a considerable efficiency recovery. As these tracks are independent of NDC1, the total efficiency ($3D$-$3D$ + $2D$-$3D$ + $vertex$-$3D$) is nearly model independent.

[a] The chambers had a superior performance in NOMAD (95% hit efficiency and a resolution a factor of two better). This is mainly due to the use of different non-flammable gas mixture $(Ar(90\%) - CO_2(9\%) - CH_4(1\%))$, and volatage settings (sense wires held at +1300V and potential wires at -2900V). However, one should stress that this spatial resolution is more than sufficient for HARP physics

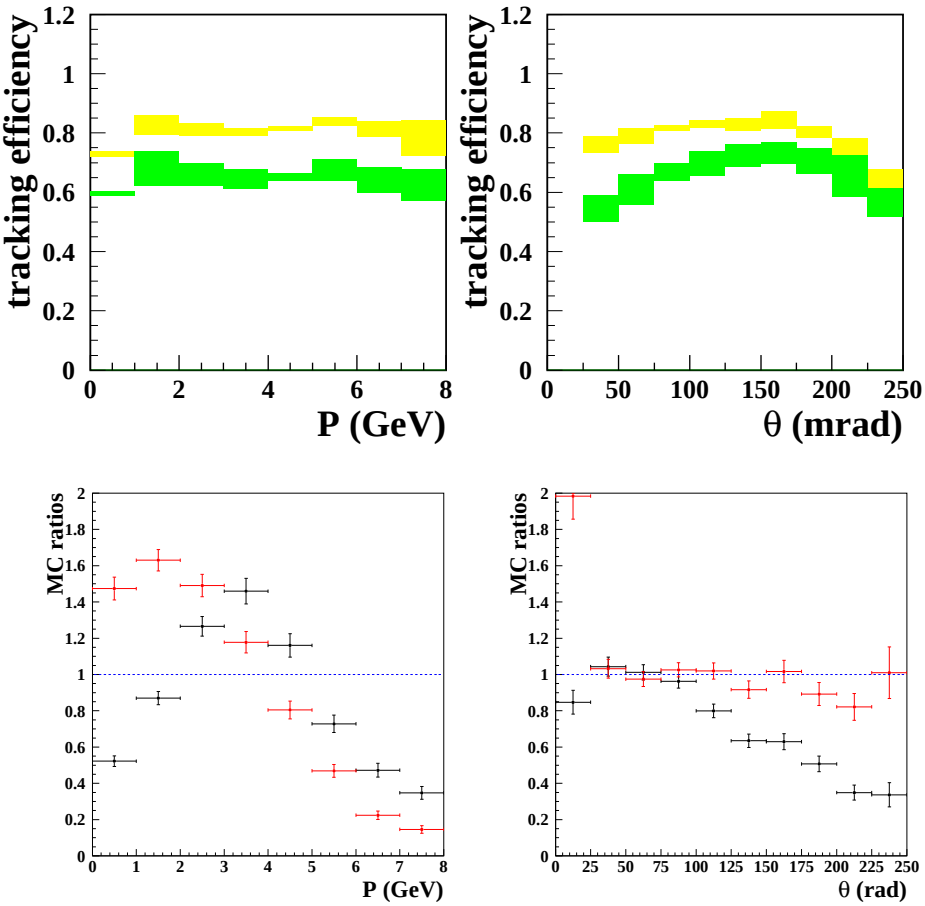

Figure 3: On the top, tracking efficiency as a function of momentum (left) and angle (right). The bands represent the maximum difference between 3 Monte Carlo hadron generators (MC1, MC2, MC3). The lower band corresponds to $3D$-$3D$ up-down matches while the upper band includes also $2D$-$3D$ up-down matches. On the bottom, the ratio between the p and θ distributions of secondary particles produced by the different hadron generators. The two sets of points correspond to the ratios MC2/MC1 and MC3/MC1.

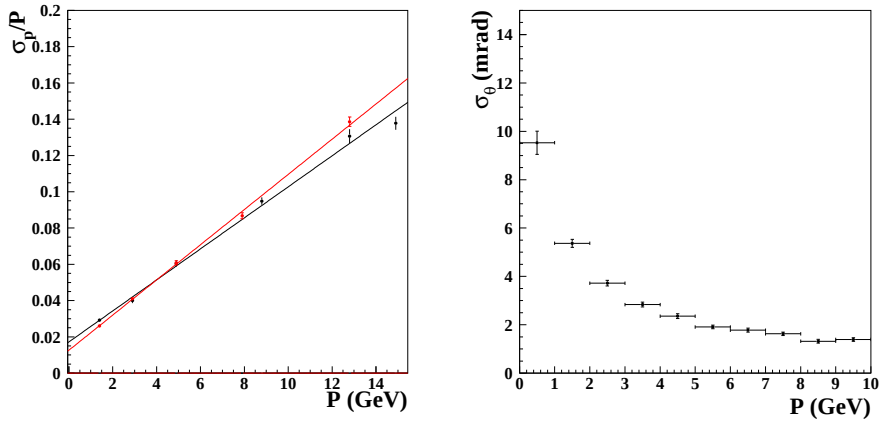

Figure 4: On the left, momentum resolution for data (dark) and Monte Carlo (light). On the right, angular resolution for Monte Carlo. Both correspond to $3D$-$3D$ matches, with no vertex constraint included.

4 Particle Identification

Particle identification in HARP's forward region uses the information from the time of flight system (TOF), the threshold cerenkov (CKOV) and the electron identifier (EID). Pion/proton separation is provided by TOF up to 4.5 GeV/c, and by the CKOV above 3 GeV/c. Electron/pion separation is covered by the CKOV below 3 GeV/c and by the EID above 2 GeV/c. Finally the kaon contamination can be estimated with the CKOV above 3 GeV/c and with the (TOF) below this energy.

4.1 Time of flight System

Particle identification by time of flight in HARP's forward region relies on the combination of particle momenta (p) and track length (L), measured with the forward spectrometer, and the time-of-flight between a start signal (t_0) from the beam time detectors and a stop signal (t_w) from the TOF wall, placed at about 10 meters downstream from the target. The mass of a particle can be computed from these quantities, $m^2 = p^2 \cdot [((t_w - t_0) \cdot c/L)^2 - 1]$.

A recent analysis of the recorded data shows that, after the calibration procedure, the intrinsic TOF wall resolution is of the order of 150 ps, while the t_0 resolution is close to 70 ps. However, the t_0 resolution used for the analysis shown in this paper was above 200 ps, leading to a combined TOF resolution of about 270 ps, which is already better that the design value of 300 ps.

With this TOF resolution and the current momentum resolution the TOF is able to provide a π/p separation of $\sim 5\sigma$ at 3 GeV/c, as can be seen in Fig. 5. This figure also shows the TOF performance for secondary particles in a "K2K thin target" run. In practice, the TOF system will provide reasonable π/p separation up to 4.5 GeV/c. The π/k capabilities of the detector at low energies (<3 GeV/c) are being studied at the moment [b].

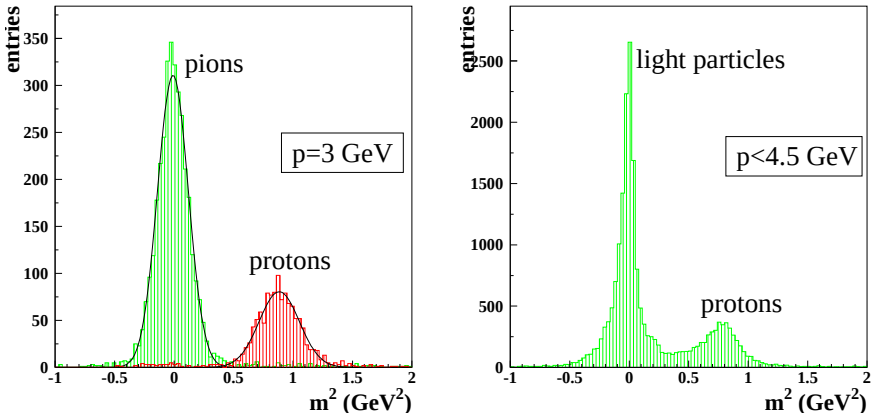

Figure 5: Mass squared as measured by the TOF system for 3 GeV/c no target data (left) and particles below 4.5 GeV/c in a 12.9 GeV/c "K2K thin target" run.

[b] It has been recently proposed to use unbiased golden events (all beam time detectors firing to gain in t_0 resolution) and tracks (crossing the overlap region between counters in the TOF wall to increase the t_w resolution) in order to estimate the π/k ratio below 3 GeV/c. The t_0 resolution obtained in this case is close to 130 ps. Anyway, the kaon contamination at these energies is known to be very small.

4.2 Threshold cerenkov

The cerenkov detector consists of a large steel frame with an opening 6 m wide and 3 m high. Two large boxes define the cerenkov vessel with a total volume of $\sim 31\ m^3$ filled with perflurobutane (C_4F_{10}). The particles traverse about 2 m of the radiating medium and generate photons that are deflected by about 135^o upwards or downwards by two large cylindrical mirrors. The light is collected by two horizontal rows of 19 photomultipliers each, one row on top and one on the bottom.

The cerenkov detector is able to identify electrons below the π saturation ($\sim 4\ GeV/c$). Pions and electrons can be separated from protons and kaons below the kaon threshold at $\sim 9\ GeV/c$, and protons can be discriminated above this energy. Fig. 6 shows the photoelectron yield for beam pions, electrons and protons in both 3 and 5 GeV/c no target runs. At 3 GeV/c we can see that π/e separation is still possible while π/p separation is quite pure but with a low efficiency. At 5 GeV/c, pions are close to the saturation regime and cannot be distinguished from electrons, which on the other had must be very rare at these energies. However, π/p separation is highly pure and efficient at 5 GeV/c (and above).

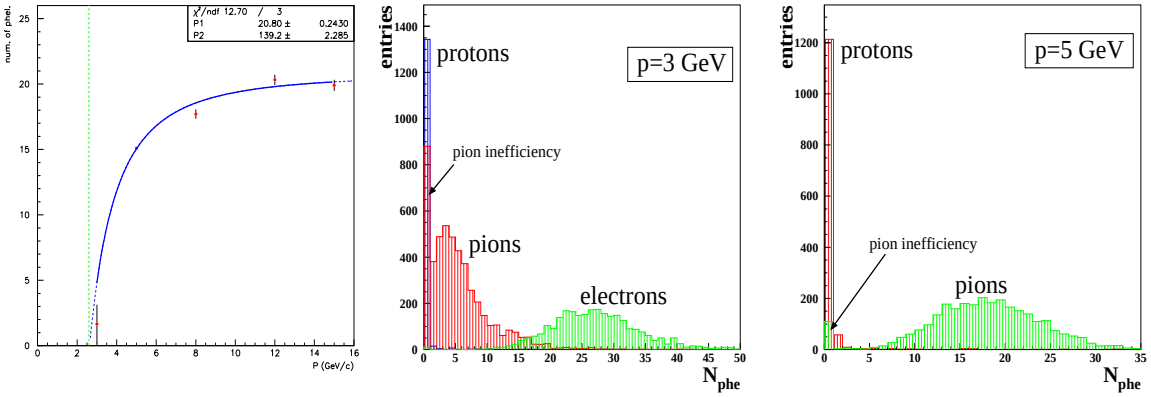

Figure 6: On the left, photoelectron yield as a function of momentum for a selected sample of pions. The experimental points are fitted to the theoretical curve $N_{phe} = N_0 \cdot [1-(1+(m/p)^2)/n^2]$, where n is the refraction index of the gas, m is the pion mass, p the momentum and N_0 the photoelectron yield in the saturation regime. The pion threshold is found to be at 2.6 GeV/c. Center and right, photoelectron yield for pions, electrons and protons at 3 and 5 GeV/c respectively. Pure samples are selected using the beam detectors.

4.3 Electron identifier

The electron identifier is made of two calorimeter planes ($EID1$ and $EID2$) reused from the CHORUS experiment and described elsewhere [3]. It was designed to provide electron-pion separation when low energy ($< 3\ GeV/c$) charged pions, accompanied by knock-on electrons, are occasionally identified as electrons by the cerenkov counter. It also serves to identify electrons at high energy, when the cerenkov has lost its pion/electron separation capabilities.

The detector performance is summarised in Fig. 7 for two different data samples: one including all the particles in an empty target run at 3 GeV/c, the other one corresponding to secondary particles in a "K2K thin target run". The figure shows the yield of particles as a function of $E_1/(E_1+E_2)$ and $(E_1+E_2)/p$, where E_1 and E_2 are the energies deposited in $EID1$ and $EID2$ respectively, and p is the momentum. Two well separated populations are clearly visible at 3 GeV/c, while in the K2K run a small electron contamination is observed.

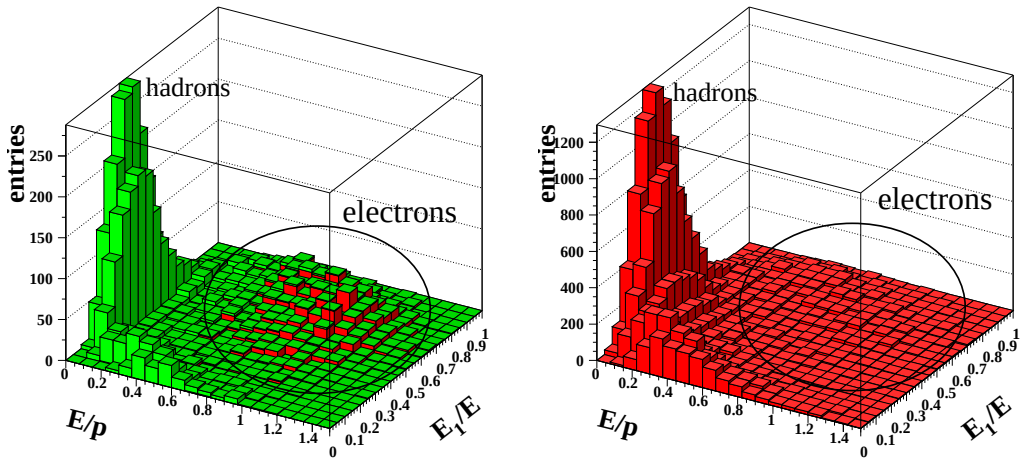

Figure 7: Particle yields as a function of E_1/E and E/p for 3 GeV/c no target (left) and 12.9 GeV/c "K2K thin target" (right). E is the total energy deposited in the calorimeter ($E_1 + E_2$).

5 The analysis

One sixth (1 million events) of the "K2K thin target" data has been analysed. The unnormalised pion production differential cross section can be computed as follows:

$$\sigma_i^\pi = \frac{1}{\varepsilon_i^{acc}} \frac{1}{\varepsilon_i^{track}} M_{ij} \frac{1}{\varepsilon_j^\pi} \eta_j^\pi \cdot N_j^\pi, \tag{1}$$

where the indices i and j correspond to true and reconstructed (p, θ) bins respectively. ε_i^{acc} is the geometrical acceptance, ε_i^{track} is the total tracking efficiency, M_{ij} is the migration matrix from reconstructed bin j to true bin i, ε_j^π is the pion identification efficiency, η_j^π is the pion purity and N_j^π is the observed pion yield. The pion purity is defined as $\eta_j^\pi = N_j^{true-\pi}/N_j^\pi = (N_j^\pi - N_j^{bkg})/N_j^\pi$, where $N_j^{true-\pi}$ is the number of true observed pions in the bin j, and N_j^{bkg} is the number of particles misidentified as pions in the same bin j. That means that η_j^π is just the probability of correct identification of a pion. The pion identification efficiency, ε_j^π is the fraction of times that a tracked pion is identified as such.

As we have seen in Sec. 4 the contamination from protons, electrons and kaons can essentially be measured using the data. This implies a small systematic error on the pion purity. The same is true for the pion efficiency, which can be estimated taking advantage of the PID redundancy of the subsystems.

Preliminary studies show a three-diagonal migration matrix, where migration is mainly due to finite momentum and angular resolutions, but not to systematic effects (momentum and angular biases, etc).

Fig. 8 shows the inclusive yield and the pion yield (N_i^π) as a function of p and θ. Fig. 9 shows the pion yield corrected by the tracking and pion identification efficiencies ($\frac{1}{\varepsilon_i^{track} \cdot \varepsilon_i^\pi} N_i^\pi$) as a function of p and θ. This figure also shows the p/π misidentification background for the TOF system, computed with three different hadron generators.

The current activities in the context of this forward analysis follow the line of recovering tracking efficiency by using the matching between the downstream tracks and the vertex. The most recent results obtained with the improved tracking are very encouraging as they are nearly model independent. This will allow a considerable reduction of the systematic error.

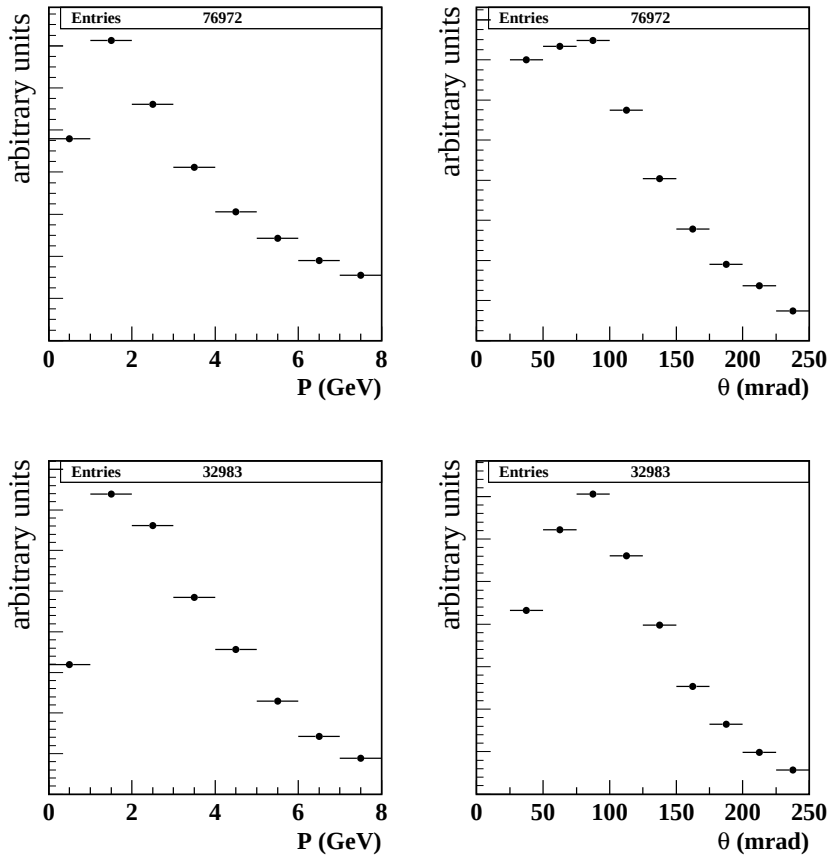

Figure 8: On the top, inclusive raw yield of charged particles as a function of p and θ. On the bottom, the raw pion yield.

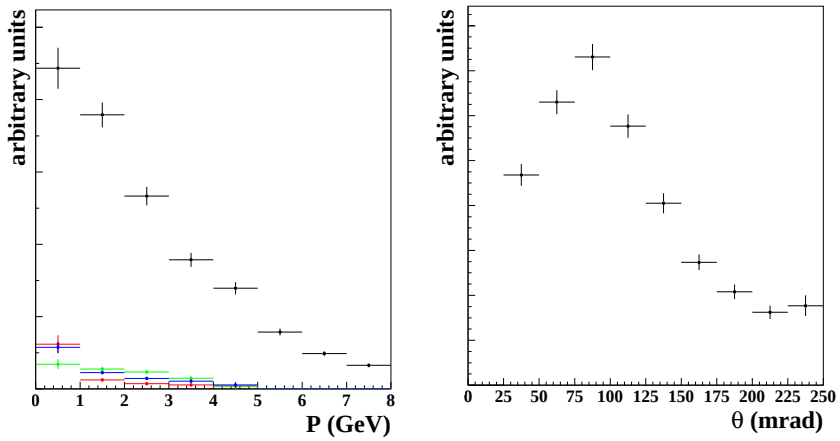

Figure 9: Raw pion yield corrected by tracking and pion identification efficiencies. On the left, the p/π misidentification background for the TOF system is also shown (for the three hadron generators). The number of Monte Carlo events used to compute the tracking efficiency was of the order of 50000. This explains the large statistical errors in these figures.

6 Conclusions

We have described the current performance of the HARP apparatus and our first physics analysis. This analysis is based on specific data taken by HARP to improve the neutrino flux calculation for the K2K experiment. Particle identification and tracking of forward going particles is well under control. This has permitted an initial estimation of the differential raw pion yield and its efficiency correction. The analysis is still in progress and will lead to conclusive results shortly.

Acknowledgments

I would like to thank the whole HARP Collaboration for their help and support. Special thanks to our K2K and MiniBooNE colleagues, Issei Kato, Linda Coney, Geoff Mills and Dave Schmitz, who have intensely collaborated to produce these results. I'm also grateful to Malcolm Ellis for his invaluable help, including the English corrections of this article.

References

1. The HARP Collaboration, CERN-SPSC/2003-027, SPSC-P-325
2. M. Anfreville *et al.*, *Nucl. Instrum. Methods* A **481**, 339 (2002).
3. The CHORUS Collaboration, *Nucl. Instrum. Methods* A **349**, 70 (1994).
   The CHORUS Collaboration,*Nucl. Instrum. Methods* A **378**, 221 (1996).
4. http://www-boone.fnal.gov/publicpages/runplan.ps.gz
5. M.H. Ahn *et al.*, The K2K Collaboration *Phys. Rev. Lett.* **490**, 041801 (2003).
   M.H. Ahn *et al.*, The K2K Collaboration *Phys. Lett.* B **511**, 178 (2001).
6. R. Frühwirth *et al.*, *Data Analysis Techniques for High-Energy Physics, second edition.* Cambridge University Press, Cambridge, 2000.
   R. Frühwirth *et al.*, *Nucl. Instrum. Methods* A **262**, 444 (1987).